ISSN 1061-933X, Colloid Journal, 2011, Vol. 73, No. 6, pp. 768–776. © Pleiades Publishing, Ltd., 2011.
Original Russian Text © A.E. Galashev, O.R. Rakhmanova, O.A. Novruzova, A.A. Galasheva, A.N. Novruzov, 2011, published in Kolloidnyi Zhurnal, 2011, Vol. 73, No. 6, pp. 772–780.

Computer Simulation of Oxygen and Nitrate Ion Absorption by Water Clusters

A. E. Galashev, O. R. Rakhmanova, O. A. Novruzova, A. A. Galasheva, and A. N. Novruzov

Institute of Industrial Ecology, Ural Division, Russian Academy of Sciences, ul. Sof'i Kovalevskoi 20, Yekaterinburg, 620990 Russia

Received December 20, 2010

Abstract—Using the molecular dynamics method, the joint absorption of oxygen and nitrate ions by water clusters is studied in terms of the polarizable model of flexible molecules. Significant fluctuations are observed in the number of hydrogen bonds in the clusters during the addition of NO_3^- ions to water–oxygen aggregates. Dielectric permittivity noticeably changes upon the addition of O_2 molecules to water clusters and nitrate ions to oxygen-containing water clusters. After the absorption of oxygen molecules and nitrate ions, water clusters markedly lose the ability to IR absorption. The Raman spectrum of a medium formed from disperse aqueous system, oxygen, and nitrate ions displays a greater number of bands than the spectrum of a system of pure water clusters.

DOI: 10.1134/S1061933X11050048

INTRODUCTION

Nitrogen is the most prevailing atmospheric element and its fraction in air is nearly 80%. Gaseous nitrogen occurs in different forms, mainly, N_2, N_2O, NO, NO_2, and NH_3. Some of these gases actively interact with rain water to yield nitrate $\left(NO_3^-\right)$ and ammonium $\left(NH_4^+\right)$ ions. Nitrates arise in the atmosphere as a result of lightning-initiated chemical reactions, photochemical oxidation in stratosphere, chemical oxidation of ammonia, NO formation in the microbial processes proceeding in soil, and the combustion of hydrocarbon fuel. The anthropogenic factors have a determining effect on the contents of nitrates and ammonia registered in rain water and atmosphere. Nitrates eliminated from the atmosphere can be transformed into elemental nitrogen via denitrification processes. Most frequently, these processes occur in soil as a result of bacterial activity. Ammonium is converted into nitrate through oxidation reactions. This mechanism is responsible for nitrogen return from ammonium ions back into atmosphere [1].

Nitrate ions can be formed due to the loss of protons by nitric acid. A nitrogen atom is surrounded by four pairs of shared electrons. The initial single electron pair is transformed into a bound pair. Two pairs form a double bond. A double bond and two single bonds are separated by a longest distance possible in a triangle. In this case, all oxygen–nitrogen bonds are almost identical and the bonding is distributed uniformly over all three oxygen atoms.

For many years, the numerical calculations of ozone concentration in the upper atmosphere were not in accordance with the experimental measurements [2]. To eliminate this discrepancy, it was assumed that there is a source of excess oxygen [3]. This source is the photoinduced dissociation of ozone under the action UV radiation with a wavelength of 200–310 nm. This reaction yields molecular oxygen occurring in the ground electron state with a strong vibrational excitation [4]. An excited oxygen molecule absorbs the additional photon and is decomposed into two oxygen atoms. However, vibration energy can be transferred to another arbitrary particle. According to the estimates [4], the presence of this additional source of atomic oxygen can increase the ozone concentration of 13–60% at a height of 36–58 km.

Our estimations demonstrated that about 18% of the total amount of atmospheric water vapor is in the state corresponding to the initial stage of condensation, i.e., in the form of clusters. Evaluation data suggest that, at the current average Earth surface humidity of 11 g/m^3, the total mass of water clusters in atmosphere is about 2.08×10^{15} kg, while the mass of atmospheric oxygen is estimated as 1.18×10^{18} kg. Thus, the oxygen mass substantially exceeds the mass of water clusters. With regard to the cluster size distribution, it can be shown that about 760 oxygen molecules correspond to one average statistical water cluster [5]. Hence, the probability of the interaction between water clusters and oxygen molecules is rather high. The oxygen content in the Earth atmosphere slowly reduces. In 1989–1994, O_2 content in the atmosphere decreased on average by 0.0002% [6]. The interaction

of O_2 with atmospheric water has not yet been studied. There are no data on the effect of NO_3^- ions on this interaction or the influence of this interaction on the planetary heat balance.

The aim of this work was to study the simultaneous interaction of water clusters with nitrate ions and oxygen molecules and to determine the character of changes in the spectral characteristics of disperse aqueous systems due to such interactions.

MOLECULAR DYNAMICS MODEL

The polarizable version of the refined TIP4P model of water [7] was used in this work. In [7], the parameters of the Lennard-Jones component of the potential were significantly changed so that the coefficients at the terms characterizing the repulsion and attraction decreased by 2.5 and 2.9 times, respectively. Moreover, in this model, the center of negative charge localization was distanced from the center of the oxygen atom by 0.0215 nm instead of previous 0.015 nm. This made it possible to correct the constant dipole moment of water molecule to 1.848 D, which corresponds to its experimental value in a gas phase. The Dang–Chang polarizable model [7] was used to describe the water–water interactions. The interactions between nitrate ions and the nitrate ion–water interactions were represented by a polarizable potential model in [8], where the potential parameters were optimized to make reproducible the hydration energy and structural properties of a solvated nitrate ion. The molecular model of NO_3^- ion represents a plane triangle with N atom in the center and three O atoms at the triangle angles. The angles between the bonds are identical and equal to 120°, while the distance is $r_{NO} = 0.122$ nm. The NO_3^- ion used in the model had an effective electric charge $q_N = -1e$ (e is the elementary electric charge) associated with the nitrogen nucleus. The quantum-mechanical calculations implemented in the Hartree–Fock approximation give the nitrate ion–water bond energy equal to 14.9 kcal/mol [9]. The pair component of the atom–atom potential, which reflects the interactions between water, oxygen, and nitrate, was represented by the Lennard-Jones and Coulomb contributions. The potential parameters used to describe these interactions are given in [8, 10]. In the molecular dynamics (MD) calculations performed in terms of the Stillinger–David polarization model [11], the potential energy U of a $(H_2O)_{50}$ cluster at $T = 140$ K was equal to –24.25 eV [12]. In the model proposed in this work, U of the $(H_2O)_{50}$ aggregate at $T = 250$ K is –23.1 eV.

Flexible models of molecules were considered. The flexibility was provided via the procedure developed within the framework of the Hamilton dynamics [13, 14]. Let us consider a diatomic molecule. Assume that atoms a and b in a molecule are separated by a distance of

$$Q = |\mathbf{r}_a - \mathbf{r}_b|,$$

where $\mathbf{r}_a$ and $\mathbf{r}_b$ are vectors determining the positions of the atoms. Let us denote the corresponding velocities as $\mathbf{v}_a$ and $\mathbf{v}_b$ and represent the reduced mass as

$$\mu = \frac{m_a m_b}{m_a + m_b}.$$

The size of the molecule presented by atoms a and b is determined by the balance of the total potential force $\mathbf{f}(\mathbf{Q}) = -\frac{\partial \mathbf{r}}{\partial \mathbf{Q}} \nabla \Phi(\mathbf{r})$, and centrifugal force $-\mu Q\omega^2$,; thus

$$-\mu Q\omega^2 - \mathbf{f}(\mathbf{r}) \frac{\partial \mathbf{r}}{\partial \mathbf{Q}} = 0,$$

where $\omega = |\mathbf{v}_a - \mathbf{v}_b|/Q$ is the angular velocity. Minimizing the contribution of each generalized coordinate to potential energy U, we obtain

$$\frac{\partial}{\partial Q_i} H(\mathbf{r}, \mathbf{v}) = \frac{\partial}{\partial Q_i} \left(\frac{1}{2} \mu_i Q_i^2 \omega_i^2 + U(\mathbf{r}) \right) = 0.$$

This method is generalized for molecules of any composition [15].

The simulation of the interaction between a $6O_2 + (H_2O)_{50}$ system and NO_3^- ions was begun with constructing a configuration composed of an equilibrium $(H_2O)_{50}$ water cluster and surrounding oxygen molecules. The initial equilibrium configurations of water clusters were obtained in separate MD calculations, in which the kinetic energy of molecules composing the cluster corresponded to a temperature of 250 K. The interaction of the water cluster with oxygen molecules and nitrate ions was studied at the same temperature. Initially, the center of a free oxygen molecule was placed at a distance of 0.6–0.7 nm from the center of a nearest water molecule in the cluster. Linear O_2 molecules were randomly oriented. As a result, each oxygen molecule was in the field of molecular interaction. The cutoff radius of the molecular interactions in the model was equal to 0.9 nm. Ions were brought to the $6O_2 + (H_2O)_{50}$ system by pairs and located in the coordinate axes on different sides of the system at a distance of no shorter than 0.6 nm from any atom of a nearest molecule. As a result, O_2 molecules and NO_3^- ions were rather uniformly arranged at the surface of the $(H_2O)_{50}$ cluster. The MD calculation was carried out with time steps $\Delta t = 0.2 \times 10^{-16}$ s. Then, the time moment at which oxygen molecules and nitrate ions were brought to the water cluster will be taken as $t = 0$. The calculation of the spectral characteristics was begun from the time moment $t = 10^5 \Delta t$ (2 ps), and the

overall calculation time was $2.5\times10^6\Delta t$ time steps. Cluster $(O_2)_6(H_2O)_{50}\left(NO_3^-\right)_i$ was formed in the course of ~$5\times10^5\Delta t$ time steps. The cluster formation was corroborated by the stable values of the total dipole moment of the above aggregate, as well as by the stable distribution of bond lengths. The average bond length $\bar{L}_b$ and the average number of bonds per water molecule $\bar{n}_b$ were determined by constructing hybrid polyhedrons (HPs) every thousand time steps. HP is an analog of the Voronoi polyhedron (VP), i.e., it is a VP, in which O atom is located in the center, while neighboring H atoms form the faces. HPs were constructed for 25 oxygen atoms located closer to the center of masses of the cluster. Thereby, the situations were excluded, in which a half-space formed by any plane passing through the HP center contains no atom and the completed HP cannot be constructed. Among the nearest neighbors found by HPs, those located at distances of no longer than 0.27 nm were selected. This distance is close to the position of the first minimum in the partial function of radial distribution $g_{OH}(r)$ for $(O_2)_6(H_2O)_{50}$ cluster. The equations for the motion of molecular centers of masses were integrated by the fourth-order Gear method [16]. The motion equations for molecular rotation were analytically solved using the Rodrigue–Hamilton parameters [17], and the scheme of integration of motion equations in the presence of rotation corresponded to the approach proposed by Sonnenschein [18]. The calculations were performed with an Intel Core 2 Quad four-core computer equipped with a processor operating at clock frequency of 2.83 GHz.

DIELECTRIC PROPERTIES

Dielectric permittivity ε(ω) as a function of frequency ω was expressed by complex quantity $\varepsilon(\omega) = \varepsilon'(\omega) - i\varepsilon''(\omega)$, which was determined using the following equation [19, 20]:

$$\frac{\varepsilon(\omega)-1}{\varepsilon_0-1} = -\int_0^\infty \exp(-i\omega t)\frac{dF}{dt}dt$$
$$= 1 - i\omega\int_0^\infty \exp(-i\omega t)F(t)\,dt,$$

where ε_0 is the static dielectric permittivity and $F(t)$ is the normalized autocorrelation function of the total dipole moment of the cluster

$$F(t) = \frac{\langle \mathbf{M}(t)\cdot\mathbf{M}(0)\rangle}{\langle \mathbf{M}^2\rangle},$$

where

$$\mathbf{M}(t) = \sum_{j=1}^{N}\mathbf{d}_j(t)$$

is the sum of dipole moments of individual molecules.

Raman and IR spectra of the clusters were calculated via the autocorrelation functions of fluctuations of polarizability and dipole moment, respectively. A polar molecule is characterized by constant (gas phase) dipole moment $\mathbf{d}_{i,0}$ and polarizability tensor $\boldsymbol{\alpha}_{i,0}$. The interaction with neighboring molecules provides molecule *i* with an induced dipole moment and polarizability. In the model, each molecule can be considered as a polarizable point dipole located in the center of masses of the molecule. Dipole moment $\mathbf{d}_i$ and polarizability $\boldsymbol{\alpha}_i$ of molecule *i* are related via the interaction with the surrounding molecules [21] as follows:

$$\mathbf{d}_i = \mathbf{d}_{i,0} + \boldsymbol{\alpha}_{i,0}\sum_{j\neq i}\mathbf{T}_{ij}\mathbf{d}_j, \quad (1)$$

$$\boldsymbol{\alpha}_i = \boldsymbol{\alpha}_{i,0} + \boldsymbol{\alpha}_{i,0}\sum_{j\neq i}\mathbf{T}_{ij}\boldsymbol{\alpha}_j. \quad (2)$$

Here, $\mathbf{T}_{ij}$ is the of dipole–dipole interaction tensor

$$\mathbf{T}_{ij} = \frac{1}{|\boldsymbol{r}_{ij}|^3}\left(3\hat{\mathbf{r}}_{ij}\hat{\mathbf{r}}_{ij} - \mathbf{1}\right). \quad (3)$$

In Eq. (3), $\hat{\mathbf{r}}_{ij}$ is a unit vector having the direction $\mathbf{r}_i - \mathbf{r}_j$, where $\mathbf{r}_i$ and $\mathbf{r}_j$ are the positions of the centers of masses of molecules *i* and *j*, and denotation **1** refers to a unit tensor of the 3 × 3 rank. Anisotropic gas phase tensor of polarizability $\alpha_{xx,yy,zz} = \{1.495, 1.626, 1.286\}$ Å^3 was used for water molecules [22]. Oxygen molecules were characterized by experimental isotropic polarizability $\alpha = 1.57$ Å^3 [23]. Isotropic polarizability of NO_3^- ions was taken equal to 4.47 Å^3 [24].

Equations (1) and (2) for $\mathbf{d}_i$ and $\boldsymbol{\alpha}_i$ can be solved by matrix inversion and expressed through $\mathbf{d}_{i,0}$ and $\boldsymbol{\alpha}_{i,0}$. This calculation method yields values of $\mathbf{d}_i$ and $\boldsymbol{\alpha}_i$ in accordance with the corresponding parameters obtained by the method of iterations [7]. If the dipole moments of molecules have been determined, the cross section of IR absorption is defined as follows [21]:

$$\sigma(\omega) = \left(\frac{2}{\varepsilon_\nu c\hbar n}\right)\omega\,\mathrm{th}\left(\frac{\hbar\omega}{2kT}\right)\mathrm{Re}\int_0^\infty dt e^{i\omega t}\langle \mathbf{M}(t)\cdot\mathbf{M}(0)\rangle,$$

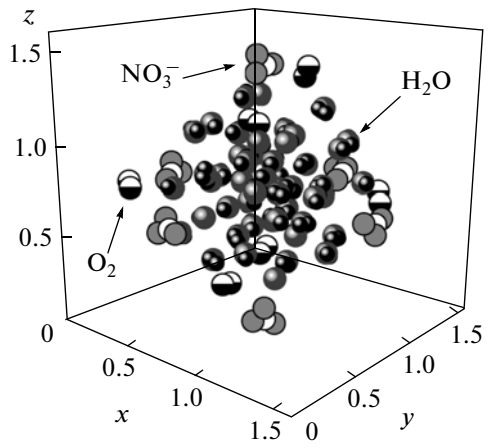

Fig. 1. Configuration of $(H_2O)_{50}(O_2)_6(NO_3^-)_6$ cluster at the 50-ps time moment. Coordinates of molecules are presented in nm.

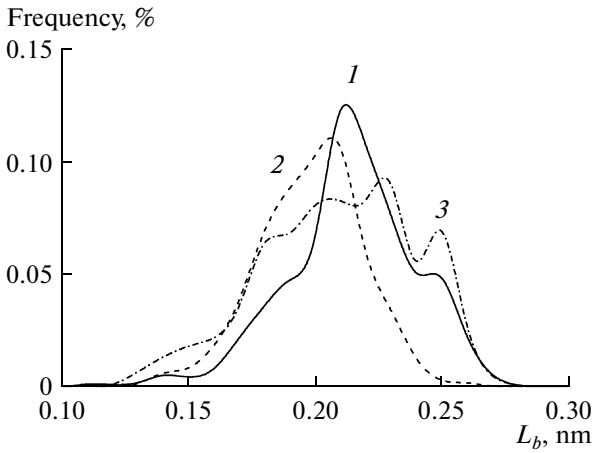

Fig. 2. Distribution of O···H bond lengths for $(H_2O)_{50} + 6O_2 + iNO_3^-$ systems: i = (*1*) 0, (*2*) 1, and (*3*) 6.

where n is the frequency-independent refractive index, ε_v is the electric constant, and c is the speed of light.

In the case of depolarized light, Raman spectrum $J(\omega)$ is determined by the following expression [21]:

$$J(\omega) = \frac{\omega}{(\omega_L - \omega)^4}\left(1 - e^{-\hbar\omega/kT}\right) \times \mathrm{Re}\int_0^\infty dt e^{i\omega t}\langle \Pi_{xz}(t)\Pi_{xz}(0)\rangle,$$

where

$$\Pi(t) \equiv \sum_{j=1}^{N}[\boldsymbol{\alpha}_j(t) - \langle\boldsymbol{\alpha}_j\rangle],$$

ω_L is the exciting laser frequency, Π_{xz} is the xz component of $\Pi(t)$, the x axis is directed along the molecular dipole, and xOy is molecular plane.

The refractive index η and the absorption coefficient of a medium ξ are determined by the following relations [25]:

$$\eta = \sqrt{\frac{\varepsilon' + \sqrt{\varepsilon'^2 + \varepsilon''^2}}{2}}, \quad \xi = \sqrt{\frac{-\varepsilon' + \sqrt{\varepsilon'^2 + \varepsilon''^2}}{2}}.$$

Coefficient ξ determines the rate of wave attenuation during its propagation in a medium. Let us define the systems as follows: (I) $(H_2O)_n$, n = 10, 15, ..., 50 and (II) $(H_2O)_{50} + 6O_2 + iNO_3^-$, i = 1, 2, ..., 6. The first and second systems comprise clusters of nine and six types, respectively.

CALCULATION RESULTS

Figure 1 shows the configuration of a system composed of a $(H_2O)_{50}$ cluster surrounded by six O_2 molecules and six NO_3^- ions obtained by the 50-ps time moment. As can be seen, both oxygen molecules and nitrate ions have noticeably approached the water cluster. Oxygen molecules, which are free of distributed charges, can approach NO_3^- ions rather close. Nitrate ions also approach water molecules at short distances to form O···H bonds. O_2 molecules retain their arbitrary orientation. NO_3^- ions are predominantly oriented under the action of one or two closest water molecules. The central part of the cluster formed from water molecules demonstrates much denser molecular packing than the periphery, which is mainly composed of NO_3^- ions and O_2. molecules.

Figure 2 illustrates the distribution of bond lengths L_b for O···H bonds formed in the $(H_2O)_{50} + 6O_2 + iNO_3^-$ systems at i = 0, 1, and 6. Every distribution has a pronounced peak in the vicinity of L_b = 0.2 nm. When adding one ion to the system, the peak is shifted from L_b = 0.212 nm to L_b = 0.206 nm. This peak is broadened with the number of NO_3^- ions in the system. In the L_b distribution of the system with i = 6, the broad peak is split into three subpeaks at L_b = 0.206, 0.227, and 0.249 nm. Moreover, a shoulder arises to the left of the first subpeak.

The connectivity of the structure of $(H_2O)_{50} + 6O_2 + iNO_3^-$ systems is characterized by the dependences of the average number of O···H bonds $\bar{n}_b$ (Fig. 3a) and the average length $\bar{L}_b$ of these bonds (Fig. 3b) on the number of NO_3^- ions. The $\bar{n}_b(i)$ function has two peaks at i = 2 and 4; the $\bar{n}_b$ value at i = 6 is lower than

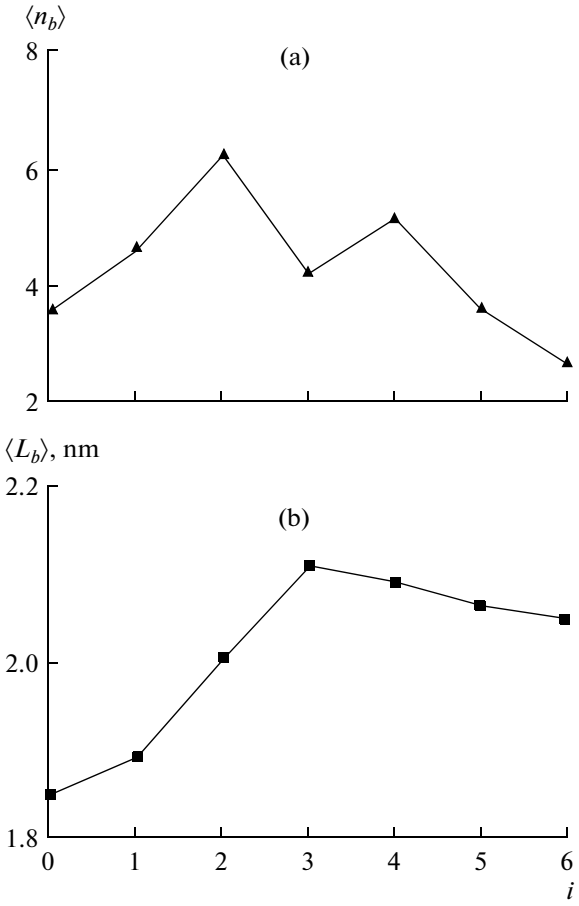

Fig. 3. (a) Average number $\bar{n}_b$ of O···H bonds and (b) average bond length $\bar{L}_b$ versus the number of NO_3^- ions in the system.

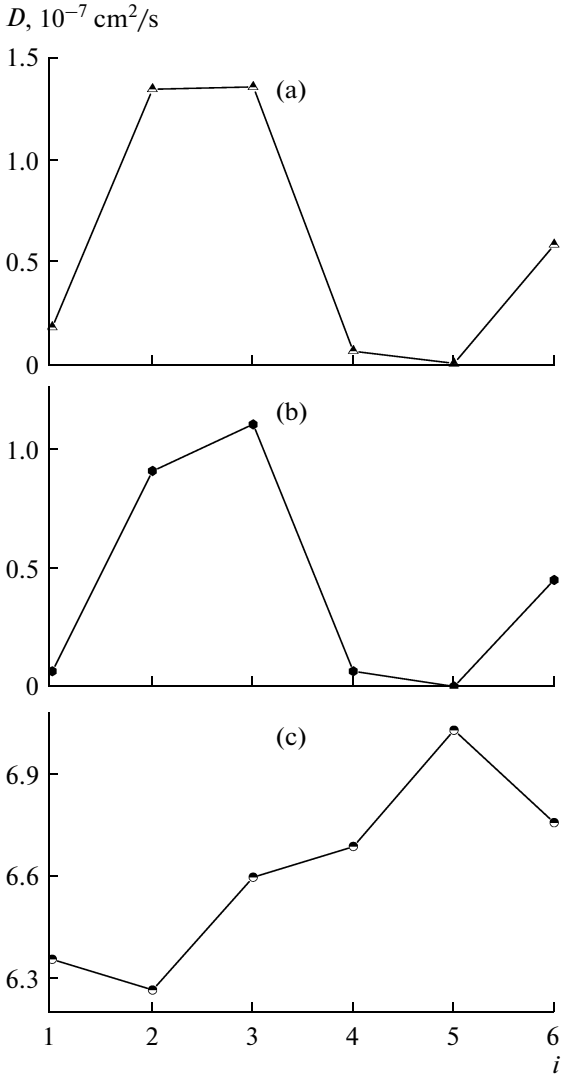

Fig. 4. Self-diffusion coefficients of (a) NO_3^- ions, (b) O_2 molecules, and (c) H_2O molecules in $(H_2O)_{50} + 6O_2 + iNO_3^-$ system versus the number of NO_3^- ions.

that at $i = 0$. Thus, at $i = 2$, the maximum number of O···H bonds is formed and, at $i = 4$, the number of bonds is also high. This is due to the densification of the system formed from H_2O and O_2 molecules under the effect of NO_3^- ions located at the opposite sides of the cluster. However, the disturbance of the water cluster also increases with the number of these pairs, and, as a result, water molecules get a higher mobility leading to the rupture of O···H bonds. Unlike the $\bar{n}_b(i)$ function, the $\bar{L}_b(i)$ dependence has a smoother shape. After the addition of the first ion to the system $\bar{L}_b$ increases, though insignificantly. The further addition of NO_3^- ions leads to a rise in the $\bar{L}_b(i)$ function followed by its decrease with a weakly pronounced maximum at $i = 3$.

Figure 4 demonstrates the dependences of the self-diffusion coefficients of molecules and ions on the number of NO_3^- ions in the system. The mobility of the ions drastically increases after the addition of the second ion to the system; its high value remains preserved upon the addition of the third ion; however, in the presence of four and five ions, it rapidly decreases (Fig. 4a). At the same time, the addition of the sixth ion enhances mobility of NO_3^- ions anew. This behavior of the $D_{NO_3^-}(i)$ function is explained by the action of electrostatic repulsion and ion shielding by water molecules. The behavior of the self-diffusion coefficient of O_2 molecules actually reproduces the $D_{NO_3^-}(i)$ dependence (Fig. 4b). Thus, the mobility of the nonpolar molecules is completely determined by collisions with NO_3^- ions. For polar molecules, the direct dependence of their mobility on the character of motion of NO_3^- ions disappears. Water molecules, which are lighter than NO_3^- ions and O_2 molecules, have considerably higher self-diffusion coefficient. In general, the

mobility of water molecules grows with the number of NO_3^- ions in the system (Fig. 4c). The maximum of the $D_{H_2O}(i)$ dependence is observed at $i = 5$. At $i = 6$, the D_{H_2O} decreases by 3.8% relative to its maximum value. The decrease is due to the addition of an ion paired with the center located in one of the coordinate axes. The presence of a pair of ions located at the opposite sides of the aggregate causes an additional compression of the water cluster and, hence, a reduction in the mobility of D_{H_2O} molecules.

Figure 5 shows the frequency dependences of the real and imaginary components of the dielectric permittivity of systems I (curve *1*) and II (curve *3*) along with ε' and ε" values for the system of clusters $(O_2)_i(H_2O)_{50}$, $i = 1, ..., 6$ (curve *2*) and corresponding characteristics of liquid water (curve *4*). The absorption of oxygen molecules by the $(H_2O)_{50}$ cluster reduces the values of the $\varepsilon'(\omega)$ function at frequencies $\omega < 2500$ cm^{-1} and the $\varepsilon''(\omega)$ function at $\omega < 1500$ cm^{-1}; at higher frequencies, oscillations in this function are observed. The presence of NO_3^- ions in the system of clusters containing water and oxygen leads to the straightening of the $\varepsilon'(\omega)$ function at $\omega > 200$ cm^{-1} and to an increase in its values at higher frequencies. Moreover, the $\varepsilon''(\omega)$ function becomes descending at $\omega > 1000$ cm^{-1}. The smoothing of functions ε' and ε" for system II occurs due to the densification of the clusters under the influence of repulsing NO_3^-. ions. In the majority of the frequency range under consideration, the ε' and ε" functions for liquid water [26, 27] have lower values than those for the cluster systems.

Figure 6 exhibits IR absorption spectra for systems I and II along with the spectrum for liquid water [28] and the measured IR spectra of stratospheric O_2 [29] and HNO_3 [30]. The positions of the most intense bands in the IR spectra of water clusters (system I) and liquid water (3389 and 3404 cm^{-1}) are in a good accordance. The presence of NO_3^- ions and O_2 molecules in the cluster system shifts the most intense absorption band toward lower frequencies. The most intense band in the IR spectrum of liquid water represents the superposition of three modes: symmetric stretching vibrations ν_1, asymmetric stretching vibrations ν_3, and the overtone of deformation vibrations ν_2 (bending of covalent bonds). A band at 1644 cm^{-1} is due to ν_2 mode. A band at 690 cm^{-1} is due to librations resulting from limitations imposed by hydrogen bonding. A weak band at 200 cm^{-1} is determined by translational vibrations including the stretching and bending of O–H···O hydrogen bonds. The IR spectrum of the system of water clusters displays a blue shift of the libration mode by ≈380 cm^{-1} relative to the corresponding band in the IR spectrum of bulk water. The above spectral band of system I is located between the second and

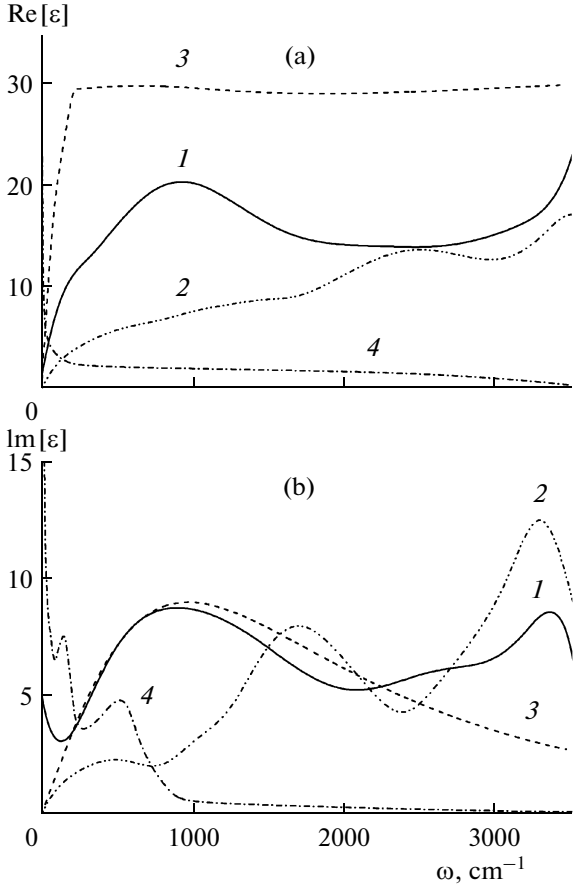

Fig. 5. Frequency dependences of (a) real and (b) imaginary components of dielectric permittivity for different systems: (*1*) $(H_2O)_n$, $10 \le n \le 50$; (*2*) $(H_2O)_{50}(O_2)_i$, $1 \le i \le 6$; (*3*) $(H_2O)_{50} + 6O_2 + iNO_3^-$, $1 \le i \le 6$; and (*4*) dada on liquid water (a) calculated by the MD method [26] and (b)experimentally measured [27].

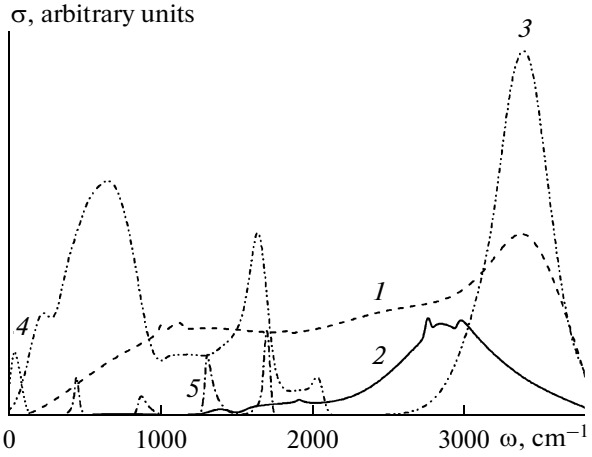

Fig. 6. IR absorption spectra for different systems: (*1*) $(H_2O)_n$, $10 \le n \le 50$; (*2*) $(H_2O)_{50} + 6O_2 + iNO_3^-$, $1 \le i \le 6$; (*3*) liquid water, experiment [28]; and (*4*, *5*) stratospheric measurements of absorption of O_2 [29] and HNO_3 [30], respectively.

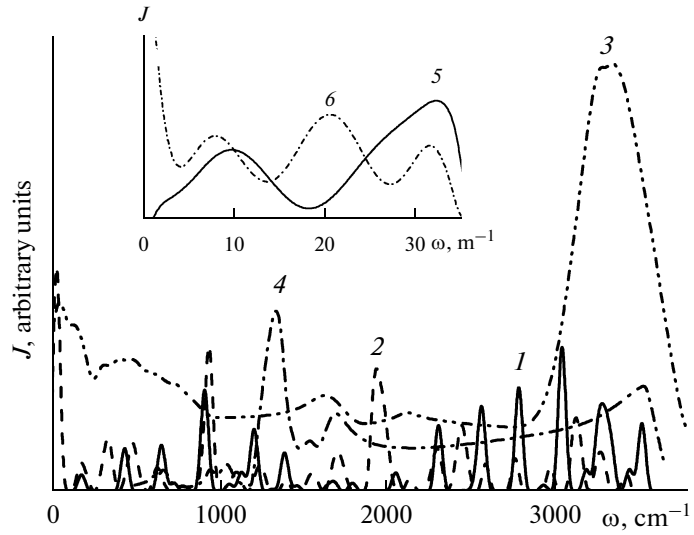

Fig. 7. Raman spectra for different systems: (*1*) $(H_2O)_n$, $10 \le n \le 50$; (*2*) $(H_2O)_{50} + 6O_2 + iNO_3^-$, $1 \le i \le 6$; (*3*) liquid water, experiment [32]; and (*4*) NO_3^-, N_2O_4 complexes in 78% aqueous HNO_3 solution [33].

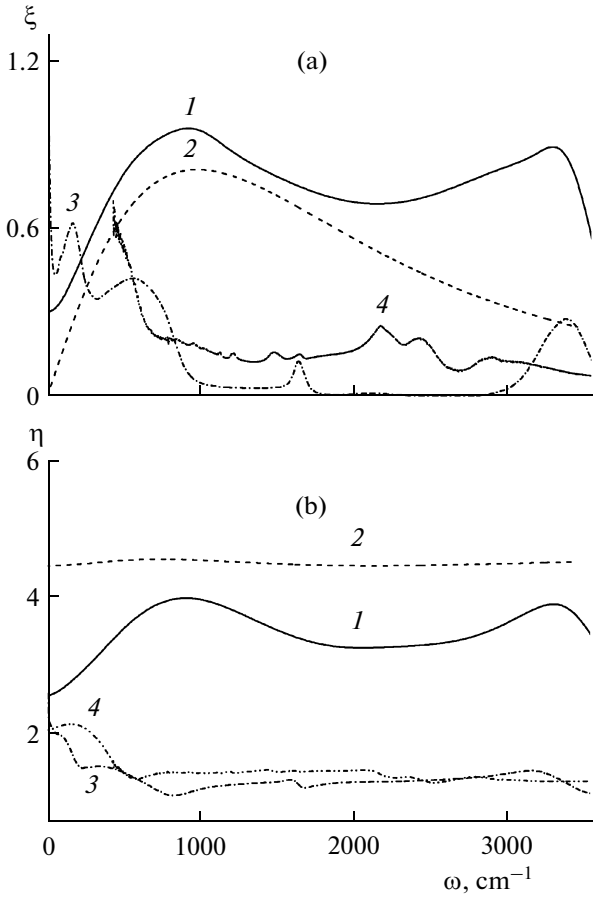

Fig. 8. Frequency dependences of (a) absorption coefficient and (b) refractive index for different systems: (*1*) $(H_2O)_n$, $10 \le n \le 50$; (*2*) $(H_2O)_{50} + 6O_2 + iNO_3^-$, $1 \le i \le 6$; and (*3*) experimental data for liquid water [34] and HNO_3 [35].

third peaks in the IR spectrum of stratospheric HNO_3, and a broad band of system II with a lower intensity is observed between the third and fourth peaks of the HNO_3 spectrum. The first low-intensity band for system II is located at 1404 cm^{-1}; its position is in good agreement with the experimentally found position (1404 cm^{-1}) of the mode of asymmetric stretching vibrations in NO_3^-/H_2O complex [31]. The third (most intense) band for the system of water clusters containing O_2 molecules and NO_3^- ions undergoes a red shift relative to the most intense band in the IR spectrum of system I. Two subpeaks in this region of system II spectrum are located at 2767 and 2825 cm^{-1}. An absorption band in the region of ≈50 cm^{-1} for stratospheric oxygen is attributed to translational vibrations resulting from the translational molecular motion.

The Raman spectra of systems I and II display a number of well-resolved peaks (Fig. 7); the most intense of them are observed at 3043 (system I) and 945 cm^{-1} (system II). The Raman spectrum of liquid water shows the most intense band at 3337 cm^{-1} [32], and Raman spectra of complexes of NO_3^-, N_2O_4 in a 78% aqueous HNO_3 solution demonstrate a band at 1350 cm^{-1} [33]. The approximation of calculated *J* spectra by a ninth-order polynomial is shown in the inset of this figure. Here, curve *5* represents the averaged Raman spectrum of system I, and curve *6* is the analogous *J* spectrum of system II. The continuity of the experimental Raman spectrum of water is related to the overlapping of bands due to reorientation of molecular dipoles around hydrogen bonds. To some extent, the averaging caused by the presentation of the *J* spectra as polynomials reflects the transition to a sys-

tem in which many clusters are observed over a long time interval. In this approach, the characteristic frequencies for system I are at 994 and 3237 cm^{-1}, and, for system II, at 810, 2065, and 3153 cm^{-1}. With regard to the anharmonicity of vibrations, the data can be interpreted as follows. Peaks at high frequencies (3237 and 3153 cm^{-1}) are due to overtones of the mode of intense longitudinal vibrations arising in liquid water at 273 K as the most intense (second) band at 686.3 cm^{-1}. The first band due to the mode of longitudinal vibrations is observed for water at 395.5 cm^{-1}. It is likely that the former bands of the averaged Raman spectra (994 and 810 cm^{-1}) reflect the overtones of this mode. A band at 2065 cm^{-1} in the *J* spectrum of system II can be interpreted as an analog of the mode (2125 cm^{-1}) in liquid water resulting from the combination of bending vibration mode ν_2 and libration modes.

The optical properties of small particles are usually determined by their refractive indices and absorption coefficients. These characteristics can hardly be obtained from the experimental IR spectra, because the measurements are often carried out with thin films. The knowledge of particle size and shape is necessary to obtain precise optical constants. Incorrect information on these characteristics leads to significant errors in the determination of the optical properties. Figure 8 shows the optical constants ξ and η calculated for systems I and II along with their experimental values for liquid water [34] and nitric acid [35]. It is evident that, throughout the frequency range, coefficient ξ for the system of pure water clusters is higher than that for $(H_2O)_{50} + 6O_2 + iNO_3^-$ system. Coefficient ξ determines the rate of electromagnetic wave attenuation in the course of its propagation. Hence, at all frequencies under consideration, the wave-attenuation rate is higher in system I compared to system II. The refractive index is the measure of the substance ability to deviate incident light rays. Index η is equal to the ratio of phase speeds of light (electromagnetic waves) in vacuum and in the given medium. Refractive index η is, on the contrary, higher in system II than in system I, i.e., system II has a higher optical density compared to system I. Moreover, the refractive index of system II is weakly dependent on frequency. Actually, in all cases, coefficients ξ for the cluster systems are higher than the values for liquid water or nitric acid at $\omega > 273$ cm^{-1}, while index ξ of the cluster systems is higher than those for liquid H_2O and HNO_3 at all considered frequencies. Hence, in the cluster systems, the propagation rate of IR radiation is significantly reduced.

CONCLUSIONS

Nitrate ions are components of atmospheric aerosols; they play an important role in many atmospheric chemical processes. The physicochemical properties of aqueous aerosols are, in many respects, dependent on the number and positions of ion. The average length of O···H bonds in water clusters adsorbing oxygen and nitrate ions reaches the maximum after the addition of three ions, and the largest number of hydrogen bonds is observed in the presence of two nitrate ions. As a rule, the mobility of water molecules increases with the number of ions in a cluster. As was shown in this work, the surface solvation of nitrate anions obviously dominates over the bulk solvation. Water clusters with adsorbed O_2 molecules and NO_3^- ions contribute to IR absorption. However, their absorbance is noticeably reduced relative to water clusters with the same number of H_2O molecules. The most intense band in the IR spectrum of a disperse aqueous system containing oxygen and nitrate ions shows a red shift relative to the corresponding spectral band for a disperse system formed from pure water clusters. The averaged Raman spectrum of these systems displays closely located bands. Moreover, the Raman spectrum of the disperse aqueous system containing O_2 molecules and NO_3^- ions demonstrates a band characteristic of liquid water, with this band being absent in the system of pure water clusters. In cluster systems, the most intense attenuation of electromagnetic waves is observed in the region of 1000 cm^{-1}. At higher frequencies, absorption of oxygen and nitrate ions results in a persistent decrease in the absorption coefficient of a disperse aqueous medium. Disperse oxygen–nitrate aqueous systems are characterized by a high refractive index weakly dependent on frequency.

Thus, in the presence of oxygen, nitrate ions are capable of absorption by water clusters in large amounts with subsequent formation of aggregates of dilute nitric acid. This process is accompanied by essential changes in the spectral characteristics and optical properties of the clusters.

ACKNOWLEDGMENTS

This work was supported by the Russian Foundation for Basic Research, project no. 08-08-00136-a.

REFERENCES

1. Berner, E. and Berner, R., *The Global Water Cycle*, New Jersey: Prentice Hall, 1987, p. 102.
2. Butler, D.M., *Geophys. Res. Lett.*, 1978, vol. 5, p. 769.
3. Slanger, T.G., Jusinski, L.E., Black, G., and Gadd, G.E., *Science* (Washington, D. C.), 1988, vol. 241, p. 945.
4. Kinugawa, T., Sato, T., Arikawa, T., Matsumi, Y., and Kawasaki, M., *J. Chem. Phys.*, 1990, vol. 93, p. 3289.
5. Galashev, A.E., *Teplofiz. Vys. Temp.*, 2010, vol. 48, p. 544.
6. Keeling, R.F., Piper, S.C., and Heimann, M., *Nature* (London), 1996, vol. 381, p. 218.

7. Dang, L.X. and Chang, T.-M., *J. Chem. Phys.*, 1997, vol. 106, p. 8149.
8. Dang, L.X., Chang, T.-M., Roeselova, M., Garrett, B.C., and Tobias, D.J., *J. Chem. Phys.*, 2006, vol. 124, p. 066101.
9. Shen, M., Xie, Y., Schaefer, H.F., and Deakyne, C.A., *J. Chem. Phys.*, 1990, vol. 93, p. 3379.
10. Hunt, S.W., Roeselova, M., Wang, W., et al., *J. Phys. Chem.*, 2004, vol. 108, p. 11559.
11. Stillinger, F.H. and David, C.W., *J. Chem. Phys.*, 1978, vol. 69, p. 1473.
12. Vostrikov, A.A., Dubov, D.Yu., and Drozdov, S.V., *Pis'ma Zh. Tekh. Fiz.*, 2008, vol. 34, p. 87.
13. Lemberg, H.L. and Stillinger, F.H., *J. Chem. Phys.*, 1975, vol. 62, p. 1677.
14. Rahman, A., Stillinger, F.H., and Lemberg, H.L., *J. Chem. Phys.*, 1975, vol. 63, p. 5223.
15. Saint-Martin, H., Hess, B., and Berendsen, H.J.C., *J. Chem. Phys.*, 2004, vol. 120, p. 11133.
16. Haile, J.M., *Molecular Dynamics Simulation. Elementary Methods*, New York: Wiley, 1992.
17. Koshlyakov, V.N., *Zadachi dinamiki tverdogo tela i prikladnoi teorii giroskopov* (Problems of Solid Body Dynamics and Applied Theory of Gyroscopes), Moscow: Nauka, 1985.
18. Sonnenschein, R., *J. Comput. Phys.*, 1985, vol. 59, p. 347.
19. Bresme, F., *J. Chem. Phys.*, 2001, vol. 115, p. 7564.
20. Neumann, M., *J. Chem. Phys.*, 1985, vol. 82, p. 5663.
21. Bosma, W.B., Fried, L.E., and Mukamel, S., *J. Chem. Phys.*, 1993, vol. 98, p. 4413.
22. Huiszoon, C., *Mol. Phys.*, 1986, vol. 58, p. 865.
23. Salvador, P., Curtis, J.E., Tobias, D.J., and Jungwirth, P., *Phys. Chem. Chem. Phys.*, 2003, vol. 5, p. 3752.
24. *Spravochnik khimika. T.1* (Chemist's Handbook), Nikol'skii, B.P., Ed., Leningrad: Khimiya, 1971, vol. 1.
25. Landau, L., Lifshitz, E., and Pitaevski, L., *Electrodynamics of Continuous Media*, Oxford: Pergamon, 1984.
26. Neumann, M., *J. Chem. Phys.*, 1986, vol. 85, p. 1567.
27. Angell, C.A. and Rodgers, V., *J. Chem. Phys.*, 1984, vol. 80, p. 6245.
28. Goggin, P.L. and Carr, C., *Far Infrared Spectroscopy and Aqueous Solutions. Water and Aqueous Solutions*, Bristol: Adam Hilger, 1986, vol. 37, p. 149.
29. Krupenie, P.H., *J. Phys. Chem. Ref. Data*, 1972, vol. 1, p. 423.
30. Goldman, A., Murcray, F.J., Blatherwick, R.D., et al., *J. Geophys. Res.*, 1992, vol. 97, p. 2561.
31. Irish, D.E. and Davis, A.R., *Can. J. Chem.*, 1968, vol. 46, p. 943.
32. Vallee, P., Lafait, J., Ghomi, M., Jouanne, M., and Morhange, J.F., *J. Mol. Struct.*, 2003, vols. 651-653, p. 371.
33. Kamboures, M.A., Van der Veer, W., Gerber, R.B., and Phillips, L.F., *Phys. Chem. Chem. Phys.*, 2008, vol. 10, p. 4748.
34. Downing, H.D. and Williams, D., *J. Geophys. Res.*, 1975, vol. 80, p. 1656.
35. Biermann, U.M., Luo, B.P., and Peter, Th., *J. Phys. Chem. A*, 2000, vol. 104, p. 783.